Shape Analysis of Planar Objects with Arbitrary Topologies Using Conformal Geometry

Lok Ming Lui[1], Wei Zeng[2,3], Shing-Tung Yau[1], and Xianfeng Gu[3]

[1] Department of Mathematics, Harvard University, Cambridge, MA, USA
[2] Department of Computer Science, Wayne State University, Detroit, MI, USA
[3] Department of Computer Science, SUNY Stony Brook, Stony Brook, NY, USA

Abstract. The study of 2D shapes is a central problem in the field of computer vision. In 2D shape analysis, classification and recognition of objects from their observed silhouettes are extremely crucial and yet difficult. It usually involves an efficient representation of 2D shape space with natural metric, so that its mathematical structure can be used for further analysis. Although significant progress has been made for the study of 2D simply-connected shapes, very few works have been done on the study of 2D objects with *arbitrary topologies*. In this work, we propose a representation of general 2D domains with arbitrary topologies using *conformal geometry*. A natural metric can be defined on the proposed representation space, which gives a metric to measure dissimilarities between objects. The main idea is to map the exterior and interior of the domain conformally to unit disks and circle domains, using holomorphic 1-forms. A set of diffeomorphisms from the unit circle $\mathbb{S}^1$ to itself can be obtained, which together with the conformal modules are used to define the shape signature. We prove mathematically that our proposed signature uniquely represents shapes with arbitrary topologies. We also introduce a reconstruction algorithm to obtain shapes from their signatures. This completes our framework and allows us to move back and forth between shapes and signatures. Experiments show the efficacy of our proposed algorithm as a stable shape representation scheme.

1 Introduction

Shape analysis of objects from their observed silhouettes is important for many computer vision applications, such as classification, recognition and image retrieval. In order to perform shape analysis effectively, it is necessary to have an efficient shape representation and a robust metric measuring shape dissimilarity.

Recently, many different representations for 2D shapes and various measures of dissimilarity between them have been proposed. For example, Zhu et al. [1] proposed the representation of shapes using their medial axis and compare their skeletal graphs through a branch and bound strategy. Liu et al. [2] used shape axis trees to represent shapes, which are defined by the locus of midpoints of optimally corresponding boundary points. Belongie et al. [3] proposed to represent and match 2D shapes for object recognition, based on the shape context and the

K. Daniilidis, P. Maragos, N. Paragios (Eds.): ECCV 2010, Part V, LNCS 6315, pp. 672–686, 2010.

Hungarian method. Mokhtarian [4] introduced a multi-scale, curvature-based shape representation technique for planar curves, which is especially suitable for recognition of a noisy curve. Besides, various statistical models for shape representation were also proposed by different research groups [5,6,7]. These approaches provide a simple way to represent shapes with finite dimensional spaces, although they cannot capture all the variability of shapes. Yang et al. [8] proposed a signal representation called the Schwarz representation and applied it to shape matching problems. Lee et al. [9] proposed to represent curves using harmonic embedding through their complete silhouettes. Lipman et al. [10] proposed to detect shape dissimilarities up to isometry using conformal densities. Their works focus on simply-connected domains. Zeng et al. [11] presented to match and register 3D multiply-connected domains using holomorphic differentials. Zeng et al. [12] analyzed 3D surfaces based on conformal modules. Their shape index can only determine shapes up to conformal deformations. Mumford et al. [13] proposed a conformal approach to model simple closed curves which captured subtle variability of shapes up to scaling and translation. They also introduced a natural metric, called the Weil-Petersson metric, on the proposed representation space.

Most of the above methods work only on simple closed curves and generally cannot deal with multiply-connected objects. In real world applications, objects from their observed silhouettes are usually multiply-connected domains (i.e. domains with holes in the interior). In order to analyze such kind of shapes effectively, it is necessary to develop an algorithm which can deal with multiply-connected domains. This motivates us to look for a good representation, which is equipped with a natural metric, to model planar objects of arbitrary topologies.

In this paper, we extend Mumford's conformal approach [13], which models 2D simply-connected domains, to represent multiply-connected shapes. Mumford's approach provides an effective way to represent 2D simple curves and capture their subtle differences. To extend it to multiply-connected shapes, the key idea of our method is to map the exterior and interior of the domain conformally to unit disks and punctual disks, using holomorphic 1-forms. A set of diffeomorphisms from the unit circle $\mathbb{S}^1$ to itself can be obtained, which together with the conformal modules are used to define the shape signature. Our proposed signature uniquely represents shapes with arbitrary topologies up to scaling and translation. We also introduce a reconstruction algorithm to obtain shapes from their signatures. This completes our framework and allows us to move back and forth between shapes and signatures. The proposed representation space inherits a natural metric that can be used to measure dissimilarity between shapes.

2 Theoretically Background

In this section, we briefly introduce the theoretical foundations necessary for the current work. For more details, we refer readers to the classical books [14,15].

2.1 Beltrami Equation

Consider a complex valued function $\phi : \mathbb{C} \to \mathbb{C}$ maps the z-plane to the w-plane, where $z = x + iy$, $w = u + iv$. The *complex partial derivative* is defined as: $\frac{\partial}{\partial z} := \frac{1}{2}(\frac{\partial}{\partial x} - i\frac{\partial}{\partial y})$, $\frac{\partial}{\partial \bar{z}} = \frac{1}{2}(\frac{\partial}{\partial x} + i\frac{\partial}{\partial y})$. The *Beltrami equation* for ϕ is defined by: $\frac{\partial \phi}{\partial \bar{z}} = \mu(z)\frac{\partial \phi}{\partial z}$, where μ is called the *Beltrami coefficient*. If μ is zero, then ϕ is called a *holomorphic* or *conformal mapping*. Otherwise, if $\|\mu\|_\infty < 1$, then ϕ is called a *quasiconformal mapping*. Given a compact simply-connected domain Ω in $\mathbb{C}$ and a Beltrami coefficient μ with $\|\mu\|_\infty < 1$. There is always a quasiconformal mapping from Ω to the unit disk $\mathbb{D}$ which satisfies the Beltrami equation in the distribution sense [14].

2.2 Conformal Module

Suppose Ω_1 and Ω_2 are planar domains. We say Ω_1 and Ω_2 are *conformally equivalent* if there is a biholomorphic diffeomorphism between them. All planar domains can be classified by the conformal equivalence relation. Each conformal equivalence class shares the same *conformal invariants*, the so-called *conformal module*. The conformal module is one of the key component for us to define the unique shape signature.

Suppose Ω is a compact domain on the complex plane $\mathbb{C}$. If Ω has a single boundary component, the it is called a *simply-connected domain*. Every simply connected domain can be mapped to the unit disk conformally and all such kind of mappings differ by a *Möbius transformation*: $z \to e^{i\theta}\frac{z - z_0}{1 - \bar{z}_0 z}$.

Suppose Ω has multiple boundary components $\partial\Omega = \gamma_0 - \gamma_1 - \gamma_2 \cdots \gamma_n$, where γ_0 represents the exterior boundary component, then Ω is called a *multiply-connected domain*. A *circle domain* is a unit disk with circular holes. Two circle domains are conformally equivalent, if and only if they differ by a Möbius transformation. It turns out every multiply-connected domain can be conformally mapped to a circle domain, as described in the following theorem.

Theorem 1 (Riemann Mapping for Multiply-Connected Domain). *If Ω is a multiply-connected domain, then there exists a conformal mapping $\phi : \Omega \to D$, where D is a circle domain. Such kind of mappings differ by Möbius transformations.*

Therefore, each multiply-connected domain is conformally equivalent to a circle domain. The conformal module for a circle domain is represented as the centers and radii of inner boundary circles. All simply-connected domains are conformally equivalent. The topological annulus requires 1 parameter to represent the conformal module. In general case, because there are $n > 1$ inner circles, and the Mobius transformation group is 3 dimensional, therefore the conformal module requires $3n - 3$ parameters. We denote the conformal module of Ω as $Mod(\Omega)$. Fix n, all conformal equivalence classes form a $3n - 3$ Riemannian manifold, the *Teichmüller space*. The conformal module can be treated as the Teichmüller coordinates. The Weil-Peterson metric [13] is a Riemannian metric for Teichmüller space, which induces negative sectional curvature, therefore, the geodesic between arbitrary two points is unique.

2.3 Holomorphic Differentials

In order to compute the conformal modules, one needs to find the holomorphic differential forms on the multiply-connected domain. A *differential 1-form* on a planar domain ω is defined as $\tau = f(x,y)dx + g(x,y)dy$, where f, g are smooth functions. The *Hodge star* operator acting on a differential 1-form gives the *conjugate differential 1-form* ${}^*\tau = -g(x,y)dx + f(x,y)dy$. Intuitively, the conjugate 1-form $*\tau$ is obtained by rotating τ by a right angle everywhere.

A *holomorphic 1-form* consists of a pair of conjugate harmonic 1-forms $\omega = \tau + i\ {}^*\tau = \phi(z)dz$, where $\phi(z)$ is a holomorphic function. We further requires that either τ or ${}^*\tau$ is orthogonal to all the boundaries. All holomorphic 1-forms form a group (with real coefficients), denoted as $\mathbb{H}(\Omega)$. A basis of $\mathbb{H}(\Omega)$ is given by: $\{\omega_1, \omega_2, \cdots, \omega_n\}$, such that $\int_{\gamma_j} \omega_i = \delta_i^j$, where δ_i^j is the Kronecker symbol.

By integrating the holomorphic 1-forms, one can construct the conformal *circular slit map*, whose existence is guaranteed by the following theorem.

Theorem 2 (Circular Slit Map). *Suppose Ω is a multiply connected domain with more than one boundary components, then there exists a conformal mapping $\phi : \Omega \to \mathbb{C}$, such that γ_0, γ_1 are mapped to concentric circles, γ_k's are mapped to concentric circular slits. All such kind of mappings differ by a rotation.*

2.4 Conformal Welding

This work is built on *conformal welding*, which is constructed as follows. Suppose $\Gamma = \{\gamma_0, \gamma_1, \cdots, \gamma_k\}$ is a set of non-intersecting smooth closed curves on the complex plane. Γ segments the plane to a set of connected components $\{\Omega_0, \Omega_1, \cdots, \Omega_s\}$, each segment Ω_i is a multiply-connected domain. We assume Ω_0 contains the infinity point, $p \notin \Omega_0$. By using a Möbius transformation $\phi(z) = \frac{1}{z-p}$, p is mapped to ∞, Ω_0 is mapped to a compact domain. Replace Ω_0 by $\phi(\Omega_0)$. Construct $\phi_k : \Omega_k \to \mathbb{D}_k$ to map each segment Ω_k to a circle domain $\mathbb{D}_k$, $0 \le k \le s$. Assume $\gamma_i \in \Gamma = \Omega_j \cap \Omega_k$, then $\phi_j(\gamma_i)$ is a circular boundary on the circle domain $\mathbb{D}_j$, $\phi_k(\gamma_i)$ is a another circle on $\mathbb{D}_k$. Let $f_i|_{\mathbb{S}^1} := \phi_j \circ \phi_k^{-1}|_{\mathbb{S}^1} : \mathbb{S}^1 \to \mathbb{S}^1$ be the diffeomorphism from the circle to itself, which is called the *signature of* γ_i.

Definition 1 (Signature of a Family of Loops). *The signature of a family non-intersecting closed planar curves $\Gamma = \{\gamma_0, \gamma_1, \cdots, \gamma_k\}$ is defined as: $S(\Gamma) := \{f_0, f_1, \cdots, f_k\} \cup \{Mod(\mathbb{D}_0), Mod(\mathbb{D}_1), \cdots, Mod(\mathbb{D}_s)\}$.*

The following main theorem plays the fundamental role for the current work.

Theorem 3 (Main Theorem). *The family of smooth planar closed curves Γ is determined by its signature $S(\Gamma)$, unique up to a Möbius transformation of the Riemann sphere $\mathbb{C} \cup \{\infty\}$.*

Note that if a circle domain $\mathbb{D}_k$ is disk, its conformal module can be omitted from the signature. The Möbius transformation of the Riemann sphere is given by $(az + b)/(cz + d)$, where $ad - bc = 1, a, b, c, d \in \mathbb{C}$. The proof of Theorem 3 can be found in the Appendix.

The theorem states that the proposed signature determine shapes up to a Möbius transformation. We can further do a normalization that fixes ∞ to ∞ and that the differential carries the real positive axis at ∞ to the real positive axis at ∞, as in Mumford's paper [13]. The signature can then determine the shapes uniquely up to translation and scaling.

The shape signature $S(\Gamma)$ gives us a complete representation for the space of shapes. It inherits a natural metric. Given two shapes Γ_1 and Γ_2. Let $S(\Gamma_i) := \{f_0^i, f_1^i, \cdots, f_k^i\} \cup \{Mod(\mathbb{D}_0^i), Mod(\mathbb{D}_1^i), \cdots, Mod(\mathbb{D}_s^i)\}$ $(i = 1, 2)$. We can define a metric $d(S(\Gamma_1), S(\Gamma_2))$ between the two shape signatures using the natural metric in the Teichmuller space, such as the Weil-Petersson metric [13].

Besides, our signature is stable under geometric noise. Our algorithm depends on conformal maps from shapes to circle domains using holomorphic 1-forms. The computation of 1-forms is equivalent to solving an elliptic PDE, which is stable under the perturbation of boundary conditions. On the other hand, in theory, the change of topology will cause the change of conformal structures. Hence, our algorithm is sensitive to topological noise. In practice, after extracting the contours, we filter out the ones with length less than the threshold, which are treated as topological noise.

3 Algorithm

In this section, we describe our proposed algorithm in detail. Here, we assume a planar domain Ω is with n inner boundary components, Let the boundary of the mesh be $\partial\Omega = \gamma_0 - \gamma_1 \cdots - \gamma_n$, represented as a triangular mesh. We use v_i to denote a vertex, $[v_i, v_j]$ denote an edge, $[v_i, v_j, v_k]$ denote face. The angle at vertex v_i in triangle $[v_i, v_j, v_k]$ is denoted as θ_{jk}^i. The angle structure of the mesh is defined as the set: $A(\Omega) := \{\theta_{jk}^i, \theta_{ij}^k, \theta_{ki}^j | [v_i, v_j, v_k] \in \Omega\}$. In this work, all the following computations completely depend on the angle structure.

3.1 Shape Signatures of Planar Domains with Arbitrary Topologies

We describe the algorithm to compute the signature of Ω with n inner boundary components. The inner boundaries decompose Ω into several sub-domains Ω_k. The algorithm consists of two main steps, as follows:

- 1. Compute the conformal maps from Ω_k to circle domains D_k;
- 2. Compute the conformal modules for each sub-domain Ω_k and the signature f_{ij} for each boundary.

Step 1*: Conformal maps from Ω_k to circle domains D_k.* The conformal parameterization of Ω_k can be obtained easily by computing the circular slit map and performing the Koebe's iteration. Detailed algorithm can be found in [16].

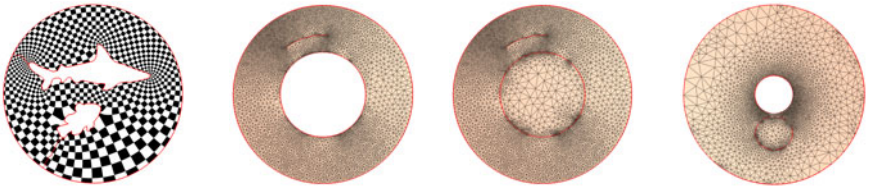

(a) Holomorphic 1-form (b) Circular slit map (c) Fill the inner hole (d) Circular map of (c)

Fig. 1. Circular slit map

Circular slit map: The circular slit map can be obtained by finding a holomorphic 1-form ω, such that

$$Img(\int_{\gamma_0} \omega) = 2\pi, \quad Img(\int_{\gamma_1} \omega) = -2\pi, \quad img(\int_{\gamma_k} \omega) = 0, \quad 2 \leq k \leq n. \tag{1}$$

To solve Equation 1, we first compute the basis for the holomorphic 1-form group. ω is then a linear combination of the basis $\omega = \sum_{k=1}^{n} \lambda_k \omega_k$, the coefficients $\{\lambda_k\}$ can be calculated by solving the linear system 1. The circular slit map is given by $\phi(p) = exp(\int_q^p \omega), \forall p \in \Omega$, where q is a base point, and the integration path is arbitrarily chosen in Ω. Figure 1 shows the circular slit map of a 2-hole planar domain.

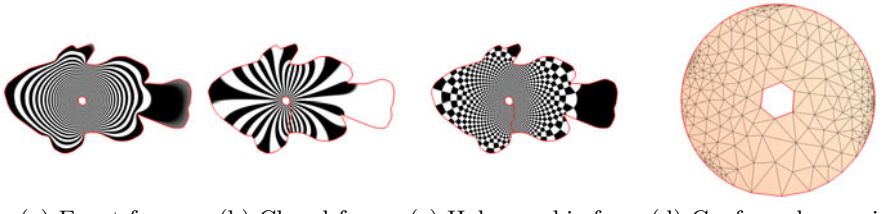

(a) Exact form (b) Closed form (c) Holomorphic form (d) Conformal mapping

Fig. 2. Conformal mapping for a simply connected domain by puncturing a small hole in the center

If Ω is a simply-connected domain (topological disk), we compute the conformal mapping to map it to the unit disk in the following way. First, we punch a small hole in the domain, and treat it as a topological annulus. Then we use circular slit map to map the punched annulus to the canonical annulus. By shrinking the size of the punched hole, the circular slit mappings converge to the conformal mapping. Figure 2 shows such an example.

Hole filling: After computing the circular slit map, the planar domain is mapped to the planar annulus with concentric circular slits. γ_0 is the unit circle, γ_1 is the inner circle, γ_k's are slits, $2 \leq k \leq n$. We use Delaunay triangulation to generate a disk D_1 bounded by γ_1, $\partial D_1 = \gamma_1$, and glue Ω with D_1 along γ_1, $\Omega_1 := \Omega \cup_{\gamma_1} D_1$. We then use circular slit map again to map Ω_1, such that

γ_2 is opened to a circle. We compute a disk D_2 bounded by γ_2, glue Ω_1 and D_2 to get Ω_2. By repeating circular slit map, at the step k, γ_k is opened to a circle. We compute a circular disk D_k bounded by γ_k, and glue Ω_{k-1} with D_k, $\Omega_k = \Omega_{k-1} \cup_{\gamma_k} D_k$. Eventually, we can fill all the holes to get Ω_n. All the disks D_k in Ω_n are not exactly circular.

Koebe's iteration: By Koebe's iteration, all the boundary components become rounder and rounder. Basically, each time, we choose a disk D_k. The complement of D_k on Ω_n is a doubly-connected domain. We map the complement to the canonical planar annulus, then γ_k becomes a circle. We recompute the disk D_k bounded by the updated γ_k, and glue the annulus with the updated D_k. After this iteration, γ_k becomes a circle. Then we choose another disk D_j, and repeat this process to make γ_j a circle. This will destroy the perfectness of the circular shape of γ_k. But by repeating this process, all the γ_k's become rounder and rounder, and eventually converge to perfect circles. The convergence is exponentially fast. Detailed proof can be found in [15].

Step 2*: Computing conformal modules and signatures f_{ij} on boundaries.* After the conformal parameterization of Ω_k to the circle domain is computed, we can compute their conformal modules and also the signature f_{ij} on each boundary. The conformal modules together with $\{f_{ij}\}$ give the complete signature $S(\Gamma)$. We demonstrate the process for computing $S(\Gamma)$ with a double fish image as shown in Figure 3. Given the original image, we first perform image segmentation to get the binary image, then calculate the contours of the objects in the image. The contour of each fish is shown in the figure. For simplicity, we treat the outermost boundary of the image as the unit circle. Then all the contours segment the image to planar domains $\Omega_0, \Omega_1, \Omega_2$. We map each planar segment to a circle domain. Ω_0 is mapped to a disk D_0 with two circular holes. The centers and radii (c_0, r_0) and (c_1, r_1) form the conformal module of Ω_0. Also, Ω_1 and Ω_2 are mapped to the unit disks D_1, D_2 respectively. We denote the conformal maps of Ω_i by $\Phi_i : \Omega_i \to D_i$. The contour of the small fish are mapped to the boundary of D_1 and one inner boundary of D_0, the signature is given by $f_{01} := \Phi_1 \circ \Phi_0^{-1}$, which is shown in frame (B) as the blue curve. Similarly, the signature f_{02} of the contour of the shark can also be computed. The signature of both fish contours is given by $S(\Gamma) = \{c_0, c_1, r_0, r_1, f_{01}, f_{02}\}$.

3.2 Reconstruction of Shapes from Signatures

Suppose Ω has n contours, then with $n+1$ segments. The signature is given by the conformal modules $\{Mod(D_k), 0 \leq k \leq n\}$ and automorphims of circles f_{ij}.

First, we construct circle domains D_k's directly from their modules $Mod(D_k)$'s. We tessellate the circular boundaries of each D_k and use Delaunay triangulation to triangulate D_k. Then, we combinatorially glue the trianglar mesh D_i and D_j by f_{ij}. Suppose the boundary circle $\gamma_i \in \partial D_i$ corresponds to $\gamma_j \in D_j$, $f_{ij} : \gamma_i \to \gamma_j$. For each vertex $v_i \in \gamma_i$, we insert $f_{ij}(v_i)$ to γ_j, vice versa, for each vertex $v_j \in \gamma_j$, we insert $f_{ij}^{-1}(v_j)$ to γ_i. Then we use constrained

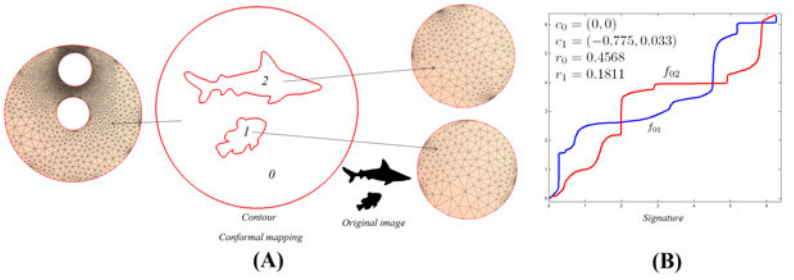

Fig. 3. Signature. Each segment is mapped to a circle domain. The conformal modules (centers and radii of inner circles) of the circle domains and the diffeomorphisms of the circles define the signature.

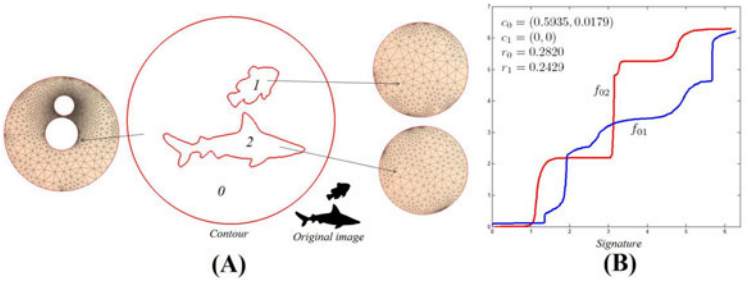

Fig. 4. The shark image with spatial changes in the positions of the two fishes. The shape signature can effectively capture spatial changes of objects in the image (compared to Figure 3).

Delaunay triangulation to refine the triangulation of D_i and D_j. Therefore the refined triangle mesh D_i and D_j can be combinatorially glued through γ_i and γ_j. We repeat this process for all f_{ij}'s, to obtain a combinatorial triangle mesh, denoted as D.

In the whole algorithm pipeline, all the computations solely depend on the angle structure. We define the angle structure of D as: $A(D) = \cup_{k=0}^{n} A(D_k)$.

Then we compute a conformal mapping ϕ from D to the unit disk using the angle structure $A(D)$. The image $\phi(D)$ differs from the original image by a Möbius transformation. This can be further removed by specifying three vertices on the outer boundary circle.

Suppose in the original image, the positions of three boundary vertices $\{v_0, v_1, v_2\}$ are $\{w_0, w_1, w_2\}$, and their positions in $\phi(D)$ are $\{z_0, z_1, z_2\}$. We need compute a unique Möbius transformation ρ, such that $\rho(z_k) = w_k$. First, we maps the unit disk to the upper half plane by $h(z) = \frac{z-i}{iz-1}$. Then on the upper half plane, we map $\{h(z_0), h(z_1), h(z_2)\}$ to $\{0, 1, \infty\}$ by $\sigma_1(z) = \frac{z-h(z_0)}{z-h(z_2)} \frac{h(z_1)-h(z_2)}{h(z_1)-h(z_0)}$. Similarly, we construct $\sigma_2(z)$, that maps $\{h(w_0), h(w_1), h(w_2)\}$ to $\{0, 1, \infty\}$. The the composition map $\sigma = h^{-1} \circ \sigma_2^{-1} \circ \sigma_1 \circ h$ is the desired Möbius transformation,

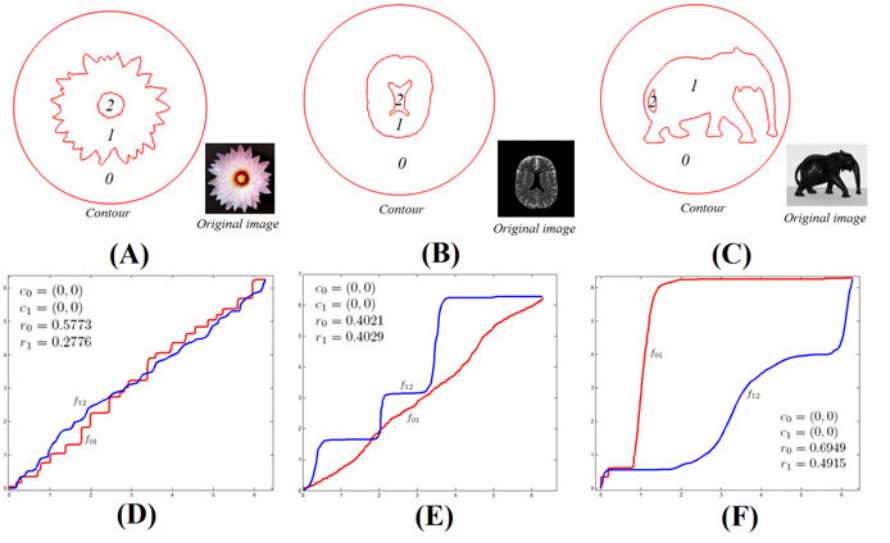

Fig. 5. Shape signatures of different images with 2 boundaries and 2 levels

which is called *normalization map*. Therefore, $\tau \circ \phi$ maps D to the unit disk, which reconstructs the contours from the signature.

4 Experimental Results

We implement our proposed algorithm using generic C++ on windows XP platform, with Intel Duo CPU 2.33 GHz, 3.98 G RAM. The numerical systems are solved using Matlab C++ library. The contour extraction is obtained by using the OpenCV library. The computational time for our algorithm is shown in Table 1. In general, both the signature calculation and reconstruction take less than 1 minute to compute, even on complicated domains.

Table 1. Computational time (second)

Model	# of contours	# of vertex	# of faces	Signature	Reconstruction
Cat	3	5247	10236	19 s	10 s
TwoCats	6	5969	11680	29 s	7 s
Ameba	2	9094	17930	8 s	12 s
Fishes	2	5978	11716	23 s	8 s
NewFishes	2	7519	14780	24 s	9 s
Elephant	2	11968	23678	17 s	-
Brain	2	8211	16164	11 s	-
Wolf	3	8451	16644	47 s	-

A. Shape Representation of Multiply-Connected Domains

Figure 4 (A) shows another double fishes image with spatial changes in the positions of the two fishes, compared with that in Figure 3. The big shark and small fish interchanged their positions. The shape signature of the image is plotted in (B), which is quite different from the shape signature in Figure 3 (see red and blue curves). In other words, our shape signature can effectively capture spatial changes of objects in the image, which can be potentially used for the purpose of image understanding. Figure 5 shows the shape signatures of 3 different images with 3 boundaries and 2 levels (levels = number of punctual disks needed for conformal parameterizations). (A) shows the shape signature of the flower image. Note that the fluctuating pattern of the outer boundary of the flower is effectively captured by f_{01} (the red curve). (B) and (C) shows the shape signatures of the brain and elephant images respectively. The three different images have very different shape signatures, meaning that our shape representation can effectively be used for classifying shapes. We also computed the shape signatures on more complicated images. Figure 6 (A) shows a wolf image with 3 boundaries and 1 level. The exterior and interior of the domain are conformally mapped to the unit disk and punctual disk. The conformal domains consist of one punctual disk with 3 inner disks removed. So, the conformal modules consist of 3 centers and 3 radii, as shown in (A). The diffeomorphisms of the unit circle on each boundary are also plotted. (B) shows the shape signature of the Mickey Mouse image with 3 boundaries and 2 levels. The conformal domain consists of two punctual disks. So, the conformal modules again consist of 3 centers and radii. The conformal modules together with the diffeomorphisms of the unit circle are plotted. Figure 7 shows an image with two cats. It consists of 6 boundaries with 2 levels. The conformal modules consist of 3 punctual disks with 3 holes removed. Hence, the conformal modules consist of 6 centers and 6 radii. The shape signatures are plotted in (B) and (C). (B) shows the signature for the outer level whereas (C) shows the signature of the inner level. Experimental results on these complicated images demonstrate the efficacy of our shape representation method.

B. Reconstruction of Shapes From Their Shape Signatures

Figure 8 shows the reconstruction of the shark image from its shape signature. The reconstructed image closely resembles to the original image, except some very tiny details are missing. The zoomed views show that the reconstructed ones are smoother, and lose the sharp corners. It shows our algorithm can effectively reconstruct shapes from their signature. We also tested our reconstruction algorithm on images with 2 levels. Figure 9 shows the Ameba image with 2 boundaries and 2 levels. The conformal domains consist of two punctual disks, each has one hole removed. The conformal modules consist of two centers and two radii. The shape signature is plotted in (B). We reconstruct the image from its shape signature in (C), which is very close to the original image. We also tested the algorithm on a more complicated example. Figure 10 shows a cat image with 3 boundaries and 2 levels. As we can see in (A), the original contour of the image is a little bit noisy. We computed the shape signature of the

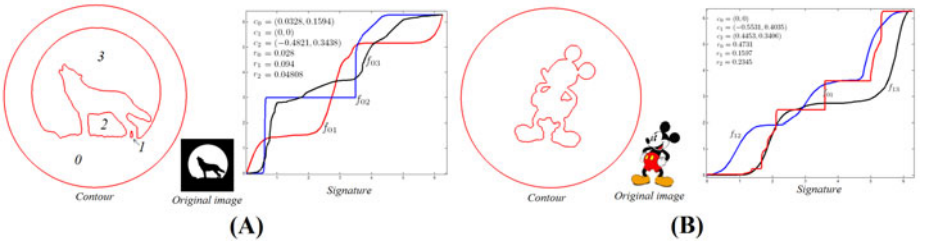

Fig. 6. Shape signatures of different images with 3 boundaries and 2 levels

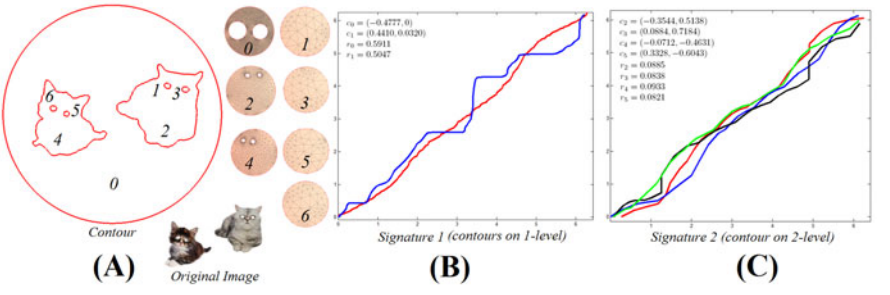

Fig. 7. Shape signatures of another image of cats with 6 boundaries and 2 levels

image, which is shown in (B). In (C), we show the reconstructed image from its shape signature. Again, the reconstructed image is very close to the original one, although the original noisy contours are smoothed out a little bit. Finally, we studied the numerical error of our reconstruction scheme. Table 2 shows the distance between the original and reconstructed contours of the Ameba and cat images. It shows a very small numerical error. The average distance is less than 0.005. It means our proposed reconstruction algorithm is very accurate.

Table 2. Distance between the original and reconstructed contours

Ameba	Number of vertex	Distance sum	Average distance
Contour 1	685	1.669626	0.002437
Contour 2	112	0.238269	0.002127
Cat	Number of vertex	Distance sum	Average distance
Contour 1	96	0.227687	0.002372
Contour 2	92	0.295533	0.003212
Contour 3	363	1.674350	0.004613

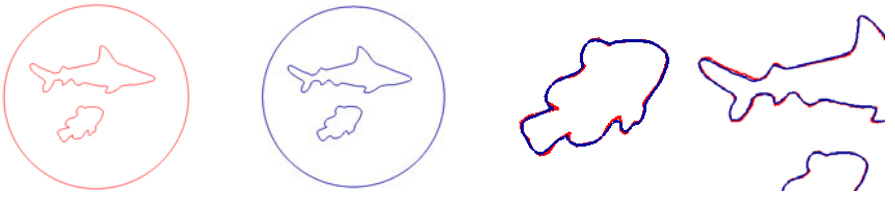

(a) Original contour (b) Reconstructed contour (c) Zoomed view (d) Zoomed view

Fig. 8. Comparison between the original contours (a) and the reconstructed ones (b). The zoomed views (c) and (d) show that the reconstructed ones are smoother

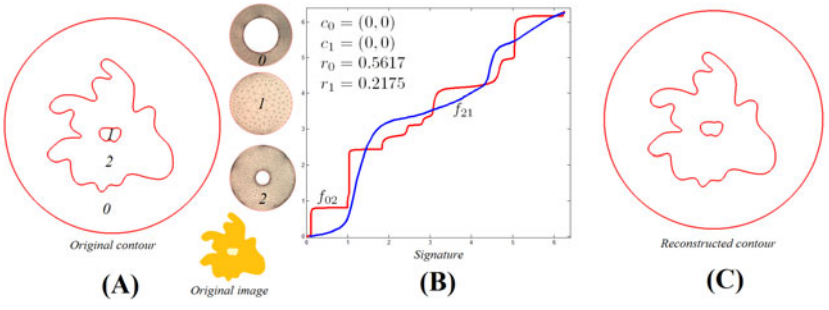

Fig. 9. Shape representation of the Ameba image and the reconstruction from its shape signature

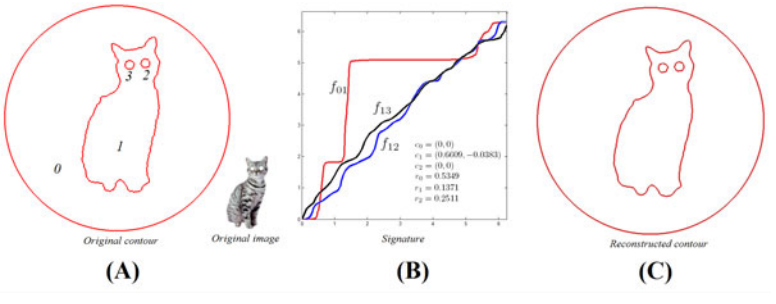

Fig. 10. Shape representation of the cat image and its reconstruction from the shape signature

5 Conclusion and Future Work

We present a shape representation of multiply-connected planar domains using conformal geometry. Using conformal geometry, a set of diffeomorphisms from the unit circle $\mathbb{S}^1$ to itself can be obtained, which together with the conformal modules are used to define the shape signature. We also introduce a reconstruction

algorithm to obtain shapes from their signatures. This completes the framework of our shape representation scheme. In the future, we will apply our algorithm for shape analysis based on Weil-Peterson metric. We will also test our proposed signatures on standard benchmark images, and compare with other existing representations for simply-connected shapes.

Acknowledgement

This work is partially supported by NIH grant R01EB0075300A1, NSF IIS 0916286, CCF0916235, CCF0830550, III0713145, and ONR N000140910228.

References

1. Zhu, S.C., Yuille, A.L.: A flexible object recognition and modeling system. IJCV 20, 8 (1996)
2. Liu, T., Geiger, D.: Approximate tree matching and shape similarity. In: ICCV, pp. 456–462 (1999)
3. Belongie, S., Malik, J., Puzicha, J.: Shape matching and object recognition using shape contexts. IEEE Trans. on Pattern Analysis and Machine Intelligence 24, 509–522 (2002)
4. Mokhtarian, F., Mackworth, A.: A therory of multiscale, curvature-based shape representation for planar curves. IEEE Trans. on Pattern Analysis and Machine Intelligence 14, 789–805 (1992)
5. Ericsson, A., Astrom, K.: An affine invariant deformable shape representation for general curves. In: Proc. IEEE Intl. Conf. on Computer Vision, vol. 2, pp. 1142–1149 (2003)
6. Sebastian, T., Klein, P., Kimia, B.: Shock based indexing into large shape databases. In: Heyden, A., Sparr, G., Nielsen, M., Johansen, P. (eds.) ECCV 2002. LNCS, vol. 2352, pp. 731–746. Springer, Heidelberg (2002)
7. Dryden, I., Mardia, K.: Statistical shape analysis. John Wiley and Son, Chichester (1998)
8. Yang, Q., Ma, S.: Matching using schwarz integrals. Pattern Recognition 32, 1039–1047 (1999)
9. Lee, S.M., Clark, N.A., Araman, P.A.: A shape representation for planar curves by shape signature harmonic embedding. In: IEEE Computer Society Conference on Computer Vision and Pattern Recognition (CVPR 2006), vol. 2, pp. 1940–1947 (2006)
10. Lipman, Y., Funkhouser, T.: Mobius Voting for Surface Correspondence. ACM Transactions on Graphics (Proc. SIGGRAPH) (August 2009)
11. Zeng, W., Zeng, Y., Wang, Y., Yin, X., Gu, X., Samaras, D.: 3D non-rigid surface matching and registration based on holomorphic differentials. In: Forsyth, D., Torr, P., Zisserman, A. (eds.) ECCV 2008, Part III. LNCS, vol. 5304, pp. 1–14. Springer, Heidelberg (2008)
12. Zeng, W., Lui, L.M., Gu, X., Yau, S.T.: Shape Analysis by Conformal Modules. Methods Appl. Anal. 15(4), 539–556 (2008)
13. Sharon, E., Mumford, D.: 2d-shape analysis using conformal mapping. International Journal of Computer Vision 70, 55–75 (2006)

14. Gardiner, F.P., Lakic, N.: Quasiconformal Teichmüler theory. American Mathematical Society, Providence (1999)
15. Henrici, P.: Applied and Computational Complex Analysis. Wiley Classics Library (1974)
16. Zeng, W., Yin, X.T., Zhang, M., Luo, F., Gu, X.: Generalized Koebe's method for conformal mapping multiply connected domains. In: SPM 2009: 2009 SIAM/ACM Joint Conference on Geometric and Physical Modeling, pp. 89–100 (2009)

Appendix: Proof of Theorem 3

Proof. See Figure 11. In the left frame, a family of planar smooth curves $\Gamma = \{\gamma_0, \cdots, \gamma_5\}$ divide the plane to segments $\{\Omega_0, \Omega_1, \cdots, \Omega_6\}$, where Ω_0 contains the ∞ point. We represent the segments and the curves as a tree in the second frame, where each node represents a segment Ω_k, each link represents a curve γ_i. If Ω_j is included by Ω_i, and Ω_i and Ω_j shares a curve γ_k, then the link γ_k in the tree connects Ω_j to Ω_i, denoted as $\gamma_k : \Omega_i \to \Omega_j$. In the third frame, each segment Ω_k is mapped conformally to a circle domain D_k by Φ_k. The signature for each closed curve γ_k is computed $f_{ij} = \Phi_i \circ \Phi_j^{-1}|_{\gamma_k}$, where $\gamma_k : \Omega_i \to \Omega_j$ in the tree. In the last frame, we construct a Riemann sphere by gluing circle domains D_k's using f_{ij}'s in the following way. The gluing process is of bottom up. We first glue the leaf nodes to their fathers. Let $\gamma_k : D_i \to D_j$, D_j be a leaf of the tree. For each point $z = re^{i\theta}$ in D_j, the *extension map*: $G_{ij}(re^{i\theta}) = re^{f_{ij}(\theta)}$.

We denote the image of D_j under G_{ij} as S_j. Then we glue S_j with D_i. By repeating this gluing procedure bottom up, we glue all leafs to their fathers. Then we prune all leaves from the tree. Then we glue all the leaves of the new tree, and prune again. By repeating this procedure, eventually, we get a tree with only the root node, then we get a Riemann sphere, denoted as S. Each circle domain D_k is mapped to a segment S_k in the last frame, by a sequence of extension maps. Suppose D_k is a circle domain, a path from the root D_0 to D_k is $\{i_0 = 0, i_1, i_2, \cdots, i_n = k\}$, then the map from $G_k : D_k \to S_k$ is given by: $G_k = G_{i_0 i_1} \circ G_{i_1 i_2} \circ \cdots \circ G_{i_{n-1} i_n}$. Note that, G_0 is identity. Then the Beltrami coefficient of $G_k^{-1} : S_k \to D_k$ can be directly computed, denoted as $\mu_k : S_k \to \mathbb{C}$. The composition $\Phi_k \circ G_k^{-1} : S_k \to \Omega_k$ maps S_k to Ω_k, because Φ_k is conformal, therefore the Beltrami coefficient of $\Phi_k \circ G_k^{-1}$ equals to μ_k.

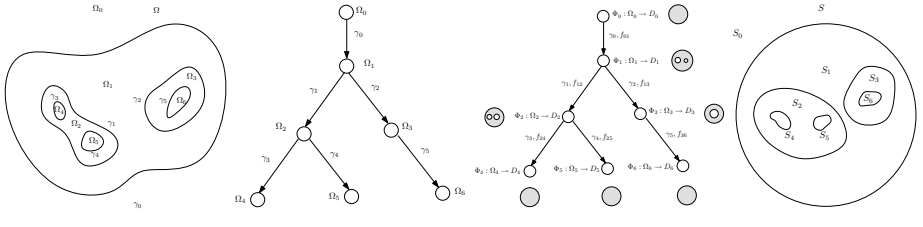

Fig. 11. Proof for the main theorem, the signature uniquely determines the family of closed curves unique up to a Mb̈oius transformation

We want to find a map from the Riemann sphere S to the original Riemann sphere Ω, $\Phi : S \to \Omega$. The Beltrami-coefficient $\mu : S \to \mathbb{C}$ is the union of μ_k's each segments: $\mu(z) = \mu_k(z), \forall z \in S_k$. The solution exists and is unique up to a Möbius transformation according to Quasi-conformal Mapping theorem [14].

Note that, the discrete computational method is more direct without explicitly solving the Beltrami equation. From the Beltrami coefficient μ, one can deform the conformal structure of S_k to that of Ω_k, under the conformal structures of Ω_k, $\Phi : S \to \Omega$ becomes a conformal mapping. The conformal structure of Ω_k is equivalent to that of D_k, therefore, one can use the conformal structure of D_k directly. In discrete case, the conformal structure is represented as the angle structure. Therefore in our algorithm, we copy the angle structures of D_k's to S, and compute the conformal map Φ directly.